Thomas Jefferson University

Annual Progress Report: 2010 Formula Grant

Reporting Period

July 1, 2013 – June 30, 2014

Formula Grant Overview

Thomas Jefferson University received $3,085,950 in formula funds for the grant award period January 1, 2011 through December 31, 2014. Accomplishments for the reporting period are described below.

Research Project 1: Project Title and Purpose

Network-Directed Therapy of Prostate Cancer - Although considerable progress has been made in the understanding of cancer genes, only a handful of molecular therapies have become standard of care for cancer patients in the last thirty years. The management of prostate cancer remains challenging, and confusion still exists regarding the molecular networks that drive the disease, the reliability of biomarkers, and the appropriateness of treatment options. The present application will address these problems taking an innovative approach. This project will focus on a single gene network, the survivin pathway, which plays a critical role in prostate cancer. This will involve analysis of tumor initiation and metastasis, *in vitro* and *in vivo*, supported by mechanistic studies on receptor ligation, gene expression, and intracellular signaling pathways.

Duration of Project

1/1/2011 – 6/30/2013

Summary of Research Completed

This project ended during a prior state fiscal year. For additional information, please refer to the Commonwealth Universal Research Enhancement C.U.R.E. Annual Reports on the Department's Tobacco Settlement/Act 77 web page at http://www.health.state.pa.us/cure.

Research Project 2: Project Title and Purpose

Cell Cycle Regulation in Prostate Cancer - In the United States, prostate cancer (PCa) is the most frequently diagnosed malignancy, and the second leading cause of cancer death, in men. The morbidity associated with this tumor type is attributed to ineffective means in combating advanced disease. Local PCa can be definitively treated by radical prostatectomy or radiation therapies. However, disseminated PCa is largely resistant to standard cytotoxic chemotherapeutics. The androgen receptor (AR) is the therapeutic target of disseminated disease. As such, first line therapies for disseminated disease are centered on the addiction of

this tumor type to androgen. This project will utilize the combined knowledge of AR and cell-cycle based cytotoxic action, to design strategies for maximal PCa cell death.

Duration of Project

1/1/2011 – 6/30/2014

Project Overview

This project builds on previous data, which show that AR activity can be effectively manipulated to sensitize cells to taxane-based cell death. The data demonstrate that the ability of AR to induce G1 progression is critical for selected cell-cycle based cytotoxic interventions. This concept will be challenged in this project, which will utilize the combined knowledge of AR and cell-cycle based cytotoxic action, to design strategies for maximal PCa cell death.

Goal: Delineate mechanisms to enhance PCa cell death through coordinated manipulation of taxane sequence, AR activity, and p53 status.

Aim 1: Determine the impact of taxanes during intermittent hormone therapy.

Aim 2: Determine the p53 requirement for androgen-enhanced taxane cytotoxicity.

Objective: These principles will challenge the impact of sequence and timing on taxane-based action during intermittent hormone therapy and the contribution of p53 status to this response.

Principal Investigator

Karen Knudsen, PhD
Associate Professor
Thomas Jefferson University
233 S. 10th Street
Philadelphia, PA 19107

Other Participating Researchers

None

Expected Research Outcomes and Benefits

This laboratory has shown that the G1-S progression function of AR sensitizes PCa cells to the cytotoxic effects of taxanes. This suggests that this function of AR could be manipulated during intermittent hormone therapy, to enhance therapeutic response and prolong or prevent tumor progression. This project addresses this innovative hypothesis directly, by dissecting the optimal cycling sequence of taxanes and AR ablative strategies using model systems reflective of naïve tumors. This research will distinguish the responses of wild-type and mutant AR. Moreover, the contribution of p53 status to this process will be determined, as taxane-induced p53 tumor suppressor activation is enhanced by active AR. Thus, the project will determine which cohorts of patients (dependent on p53 and AR status within the tumor) may most benefit from combinatorial therapy. Lastly, the ability of pharmacological agents that activate endogenous

p53 to replace or enhance the ability of AR to sensitize cells to taxanes will be determined, thus potentially identifying a novel mode of adjuvant intervention with the taxanes. Project outcomes have the capacity to markedly alter/improve therapeutic strategies to treat the most deadly forms of PCa before the stage of hormone resistance is reached.

Summary of Research Completed

Major gains have recently been realized in understanding the impact of cell cycle alterations on the response to taxane function and AR signaling in the last reporting period. Major findings are detailed below:

Cabazitaxel shows enhanced anti-proliferative and pro-cytotoxic effects in CRPC

To assess the relative impact of cabazitaxel (CBTX) and docetaxel (DCTX) on prostate cancer cell growth and survival, analyses were performed in both hormone-therapy sensitive (LNCaP) and CRPC (C4-2) model systems. Cells were treated with an increasing dose of each agent (0.1-1nM) for 48h, followed by a washout, cultured for 48h in the absence of drug, and subsequent quantification of cell viability through cell counting. As shown in Figure 1A, CBTX and DCTX showed relatively equivalent effects in hormone-therapy sensitive cells (left), with IC50 values of 0.220nM for CBTX, and 0.319nM for DCTX. However, CBTX (IC50=0.142nM) resulted in markedly enhanced anti-tumor effects as compared to DCTX (IC50=0.269nM) in CRPC cells (right). Concordantly, bivariate flow cytometric analyses monitoring both cell cycle position (via propidium iodide, PI) and progression through S-phase (via uptake of bromodeoxyuridine, BrdU) revealed a lack of S-phase entry after 16 and 48 hours of CBTX treatment in both cell types, but this was more pronounced in CRPC cells (Figure 1B, top, quantified in 1C). Similar effects were observed with DCTX (not shown), but overall effects were not as dramatic as those observed with CBTX. Thus, CBTX demonstrates an enhanced anti-proliferative effect in CRPC cells.

In addition to the observed effects on cell cycle, the sub-G1 content was enhanced in CRPC cells treated with CBTX as compared to hormone-therapy sensitive models (Figure 1B, bottom). Sub-G1 quantification revealed that CBTX is more effective in CRPC cells at inducing sub-2N DNA content (Figure 1D), eliciting almost double the effect of DCTX after 48h in C4-2 cells. Moreover, CBTX effectively induced apoptosis in C4-2 cells, as measured by PARP cleavage (not shown). Together, these data suggest that CBTX shows enhanced anti-proliferative and pro-cytotoxic effects as compared to DCTX.

Cabazitaxel promotes defective mitosis

To address the underlying means by which CBTX exhibits enhanced anti-tumor effects, the impact on nuclear integrity was assessed. Cells were fixed after 16h of exposure, and nuclear features assessed after DAPI staining (Figure 2A). Visualization on a confocal microscope demonstrated a modest enrichment of mitotic figures after 16h (quantified in Figure 2B, left), but the evidence of defective mitoses was apparent in the asymmetric appearance of segregating nuclei. Pyknotic nuclei were also observed (Figure 2A), as quantified in Figure 2B (middle), demonstrating a significant increase after 48h CBTX exposure, further supporting the contention that CBTX exerts cytotoxic effects.

Given the known function of taxanes in serving as microtubule poisons and perturbing cytoskeletal integrity, treated cells were also stained with fluorescently labeled phalloidin to visualize the cellular architecture. Actin staining revealed a reduction in cytoplasmic volume in all cells (Figure 2B). These analyses also allowed for clear definition of cell borders, revealing enhanced presence of multinucleate cells in CRPC cells treated with CBTX, likely as a result of aberrant mitosis. Multinucleate LNCaP and C4-2 cells were quantified in at least four duplicates for CBTX versus control treated samples, which demonstrated a highly significant increase in polynuclear cells after 16h and 48h (Figure 2B right). Together, these data support the hypothesis that CBTX shows an enhanced capacity to disrupt cell architecture and foster defective mitoses.

Taxane action is independent of effects on AR localization

Taxanes have been reported to affect AR localization, and could thereby potentially block prostate cancer proliferation. In previous studies, supra-clinical doses (micromolar) levels of taxanes were utilized. The *in vitro* IC50-values for these drugs, however, are in the nanomolar range. Thus, it is imperative to determine whether the reported effects occur at doses that are robustly cytostatic and cytotoxic, and are clinically attainable. As shown, using doses and time points sufficient to both suppress proliferation and induce cell death, endogenous AR remains nuclear in the presence of androgen-replete media (Figure 3A). To determine whether these effects hold true under conditions that mimic castration, parallel studies were conducted in the presence of charcoal-dextran-treated serum (CDT). As expected, androgen deprivation alone resulted in loss of nuclear AR enrichment in hormone-therapy sensitive cells; however, in CRPC cells, AR is retained in the nucleus even under castrate conditions (Figure 3B). Taken together, the enhanced cytotoxic and cytostatic effects of CBTX appear to be independent of AR subcellular regulation.

Cabazitaxel exerts enhanced anti-tumor effects in human tumors

Given desirable cytostatic and cytotoxic effects of CBTX in model systems, the anti-tumor effects were further assessed using next-generation, *ex vivo* tumor explants that allow for determination of effects on the complex 3D-tumor microenvironment. Here, fresh tumor material was obtained from radical prostatectomy of high volume disease, and tissue slices randomized into control or taxane-treated arms. As has been previously reported, these tumor slices retain the salient features of the tumor at the time of resection (including AR expression and proliferative capacity) (Figure 4A). These studies allow for intrinsically controlled analyses of taxane effects within the same tumor. Tumors were harvested after 6 days of treatment, formalin-fixed and paraffin-embedded. Standard hematoxylin and eosin (H&E) staining confirmed retention of the tumor microenvironment (Figure 4B left). Immunohistochemistry (IHC) to assess the proliferative indices (using an antibody to Ki67) was performed in parallel, for which representative examples are shown in Figure 4B (middle), and quantified in Figure 4C. Strikingly, this direct comparison in fresh tumor explants confirmed that CBTX exerts a markedly enhanced cytostatic response as compared to DCTX. Caspase-3 staining revealed an increasing trend that did not reach statistical significance, however non-significant, likely due to the limited sample number (n=3; Figure 4C). Finally, assessment of AR localization in response to drug treatment revealed retention of nuclear AR in the tumor cells (Figure 4D). Thus, similar to what was observed *in vitro*, the anti-tumor effects of CBTX appear to occur independently of altered AR localization. Collectively, these data identify an enhanced capacity of CBTX to elicit anti-proliferative and pro-apoptotic events in primary human tumors.

Tumors that progress to CRPC by RB loss show hypersensitivity to cabazitaxel

While the above studies suggest that CBTX harbors properties that are highly desirable in the clinical setting, a major hurdle is to identify tumor subtypes that would most benefit from treatment with the agent. It has been previously demonstrated that loss of retinoblastoma tumor suppressor protein (RB) or function occurs with high frequency in CRPC, and that this event alone can promote bypass of hormone therapy. By contrast, we and others have shown that RB loss compromises selected DNA damage checkpoints, and can result in sensitization to a subset of chemotherapeutics, including docetaxel. These findings put forward the provocative hypothesis that prostate cancers that achieve castration-resistance via loss of RB may be exquisitely responsive to taxanes. To assess this, isogenic pairs of LNCaP cells with control shRNA or shRNA directed against RB (shCon1 and shRB1 cells, respectively), were initially assessed *in vitro* for differential response to CBTX. In these studies, shRB1 cells demonstrated a modest sensitization to CBTX as compared to DCTX (Figure 5A). To challenge this *in vivo*, cells were subcutaneously injected into male athymic nude mice; when the xenograft tumors (n=5 per group) reached a size of 100-150mm^3, the mice were surgically castrated, allowing a week of recovery before starting 8mg/kg cabazitaxel treatment by intraperitoneal (IP) injections twice a week (Figure 5B schematic). Tumor volumes were monitored three times a week with caliper measurements, and as shown, a remarkably enhanced tumor-suppressive effect was observed in the shRB1 tumors (Figure 5B left). Normalization of individual tumor volumes at 14 days after start of treatment compared to their respective volumes at t=0 shows a significant difference in cabazitaxel response between the shCon1 tumors (n=4) and the shRB1 tumors (n=5) (Figure 5B right). Notably, the fifth mouse growing an LNCaP shCon1 tumor had to be sacrificed before this time point, because the tumor volume had already exceeded 800mm^3, despite cabazitaxel administration. These *in vivo* findings robustly support the concept that RB-deficient tumors are hypersensitive to treatment with CBTX.

To further probe the underlying basis of the observed enhanced effect in RB-deficient tumors, histopathological analyses were performed. Through H&E and Ki67 IHC analyses, shCon1 tumor cells showed expected accumulation of mitotic figures, indicating an appropriate cell cycle arrest in metaphase as a result of CBTX treatment. By contrast, shRB1 tumors elicited fewer mitotic figures (Figure 5C, quantified in 5D top), consistent with previously reported "mitotic slippage" in cells that lack cell cycle checkpoints. Quantification of Ki67 positive cells in three (40x) images per tumor slide confirmed a strong reduction in proliferative cells in the shRB1 tumors versus shCon1 (Figure 5D bottom). Taken together, the *in vivo* data suggest that RB-deficient tumors are hypersensitive to CBTX, and support the postulate that RB should be developed as a biomarker to identify tumors that may be most responsive to taxanes.

Cabazitaxel displays novel actions in prostate cancer cells by expression profiling

While the above studies identify novel anti-tumor effects of CBTX and putative biomarkers to identify tumors that would be most responsive to this taxane, additional studies were performed to further uncover the molecular basis of divergent CBTX function. Hormone therapy-sensitive cells were treated for 16h with either CBTX or DCTX, in presence or absence of steroid hormones, and subjected to a genome-wide mRNA analysis. The resulting expression data were filtered to remove low-expressing genes, to reduce background and false positive hits. Triplicate expression values were averaged, after which samples from the individual taxanes (CBTX or DCTX) were each normalized to the corresponding values for control treated samples either with

or without steroids. Differentially expressed genes were selected by a student's t-test ($p<0.05$), and compared between different treatments, as visualized by a Venn diagram (Figure 6A). Complete gene lists and fold alterations for each gene cluster have been calculated. Notably, distinct gene expression outcomes were readily apparent between the two taxanes. Further, these analyses revealed divergent effects of the agents in cells that are cycling (steroid replete) versus those that were arrested via steroid depletion (androgen deprived). These findings suggest, as expected based on the data above, that CBTX exerts differential effects as compared to DCTX, and that the proliferative status of the tumor cell can alter downstream biological effects. Genes most altered (up- or down-regulated) by cabazitaxel in absence or presence of steroids are displayed in tables in Figure 6B.

To gain deeper understanding of the cellular response to CBTX, gene ontology analyses were performed on both castrate (in yellow, corresponding to the Venn clusters in Figure 6A) and steroid replete (blue) gene lists (Figure 6B). These studies revealed enrichment of genes involved in cell cycle, M phase and mitosis exclusively after cabazitaxel treatment (Figure 6C), consistent with the enhanced anti-proliferative effect of this agent as compared to DCTX. Both drugs affect the stress-activated MAPK signaling pathway (via MAPKKK), which has been reported to play a role in taxane resistance. Under androgen-deprived conditions, CBTX and DCTX share enrichment in gene transcription related pathways. However, these appear to be negatively regulated by CBTX, versus a positive impact by DCTX, which supports the hypothesis that these drugs have distinct downstream effects. DCTX, but not CBTX, demonstrates enrichment in amino acid and protein transport regulation that could be caused by differences in microtubule stabilization. While a general mechanism has been described for taxane action, these drugs may act with differing kinetics, or be less or more efficient at stabilizing the tubulin dimers, resulting in various degrees of protein transport inhibition. The gene expression data suggest that DCTX could have a stronger effect on intracellular transport; however, the biological data suggest that this is not required for cytostatic and cytotoxic effects, and merely a bystander effect. Classical androgen receptor targets (KLK3, TMPRSS2, FKBP5, KLK2) are not affected by CBTX or DCTX, and are only altered by steroid deprivation (Figure 6D). Strikingly, the hormone conditions affect the molecular response of taxanes, as demonstrated by enrichment of distinct pathways in hormone replete versus androgen-deprived media. This differential response to CBTX (or DCTX) will likely be of relevance for designing combination therapies with androgen receptor pathway targeting drugs, such as enzalutamide and abiraterone acetate. These unbiased analyses further illustrate the divergent effects of CBTX and DCTX, and provide a gene "signature" of response to CBTX in the presence and absence of androgen.

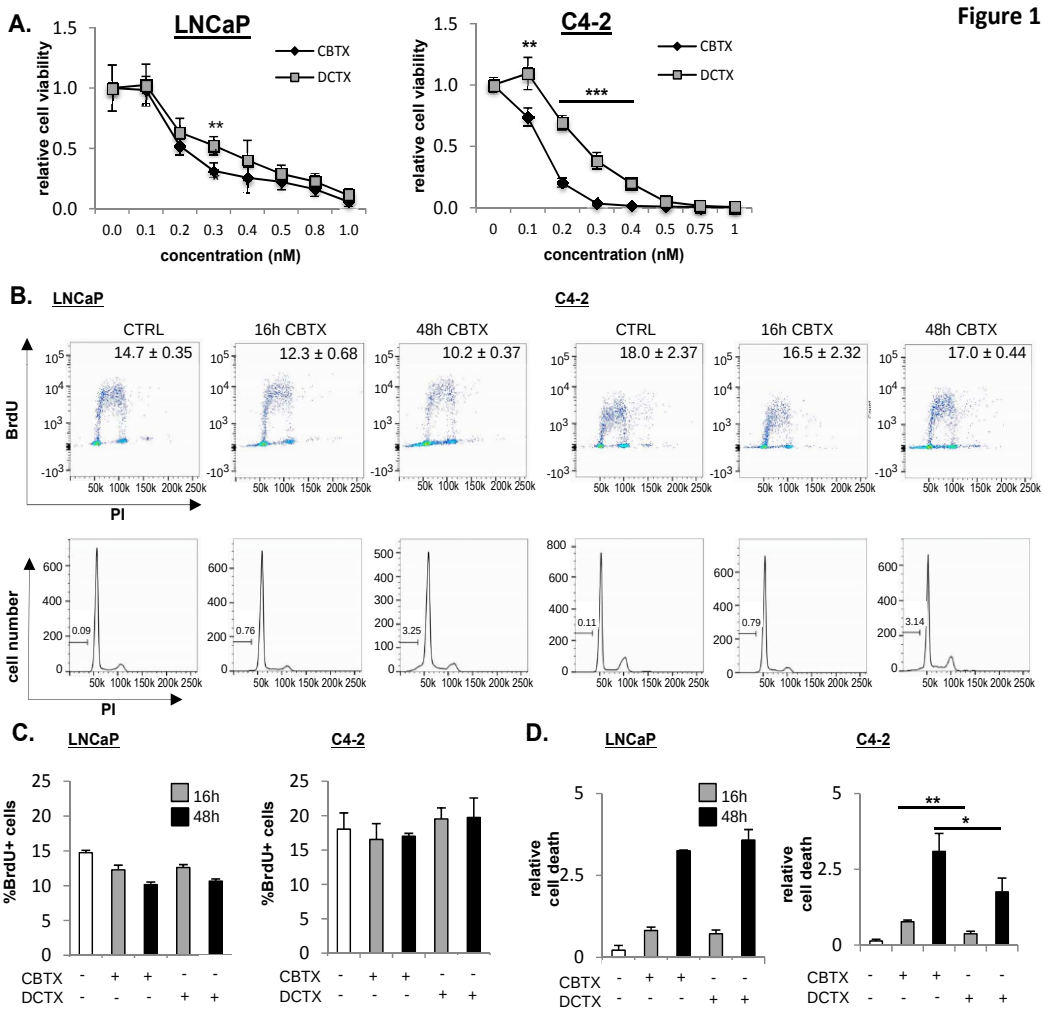

***Figure 1*: Cabazitaxel shows enhanced anti-tumor effects in CRPC.** A. Dose-dependent response to 48h cabazitaxel (CBTX) and docetaxel (DCTX) treatment and 48h fresh media without drugs was assessed in hormone therapy sensitive (LNCaP) and resistant prostate cancer cells (C4-2) by trypan blue exclusion, and cell numbers were normalized to EtOH treatment. B. Bivariate flow cytometry analyses of LNCaP and C4-2 cells treated with 1nM CBTX or control for 16 or 48h. In the top graphs, the x-axis represents relative DNA content as indicated by propidium iodide (PI) staining; the y axis shows cells undergoing active S-phase as indicated by 2h BrdU labeling. Inset values: % BrdU incorporation in viable cells (mean±s.d., from an experiment performed in biological triplicate). The bottom graphs represent the corresponding PI traces only, showing a G2M arrest, followed by cell death after CBTX exposure. C. Quantification of % BrdU+ cells in (B) and Suppl Fig 1, significant reduction is observed in taxane over control (LNCaP $p<0.05$; C4-2 $p<0.0005$ for all conditions). CBTX has a stronger effect compared to DCTX in C4-2 after 16h ($p=0.0016$). D. Taxanes induce significant cell death after 48h of CBTX or DCTX over CTRL in both LNCaP and C4-2 cells ($p<0.01$, detected as an increase in Sub-G1 content by flow cytometry (PI in B), with enhanced effects in the CRPC cells. Asterisks indicate significant differences between CBTX and DCTX at the same treatment duration, showing no significance in LNCaP, but improved efficacy for CBTX in C4-2 cells (16h 0.0042; 48h $p=0.0092$).

Figure 2

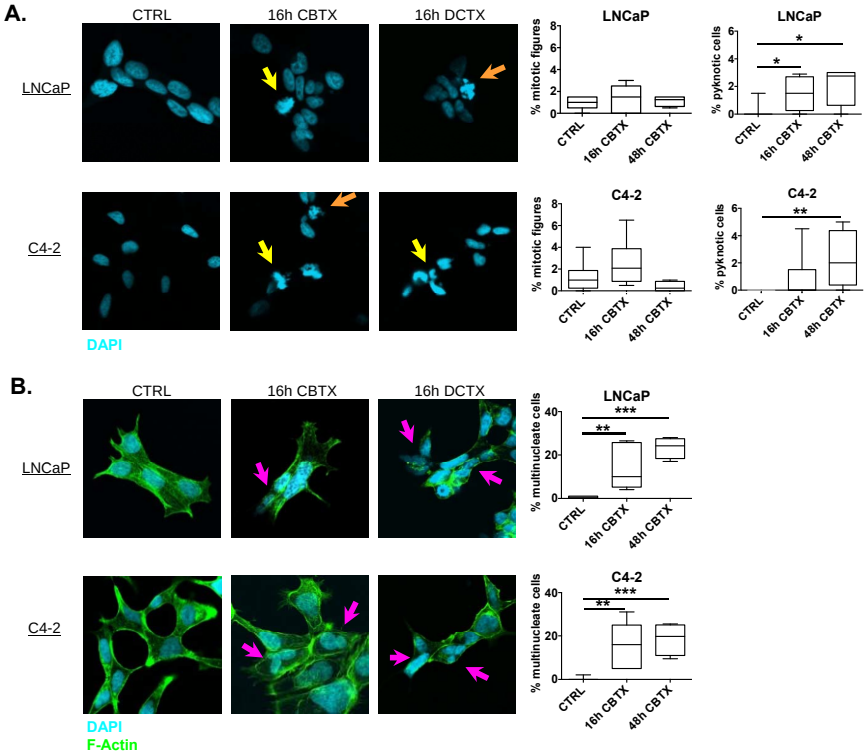

Figure 2: Cabazitaxel treatment results in increased multinucleated cells and aberrant nuclei. A. The nuclei of fixed LNCaP and C4-2 cells that were treated for 16hrs with taxanes were visualized with DAPI staining (cyan) on a confocal microscope (40x), demonstrating defective mitosis and pyknotic nuclei. B. Actin stained with Alexa Fluor 488 labeled phalloidin shows changes in cytoplasmic volume and cell morphology, as induced by taxanes after 16hrs compared to control. The zoomed images show examples of multinucleate cells in 48h treated cells, which are quantified in the whisker plots. Quantification of multinucleate cells and pyknotic cells mitotic figures in at least quadruplicate shows significant elevation of multinucleate C4-2 cells after 16h and 48h CBTX treatment, pyknotic cells after 48h. C4-2 cells show a modest, however non-significant increase in mitotic figures.

Figure 3

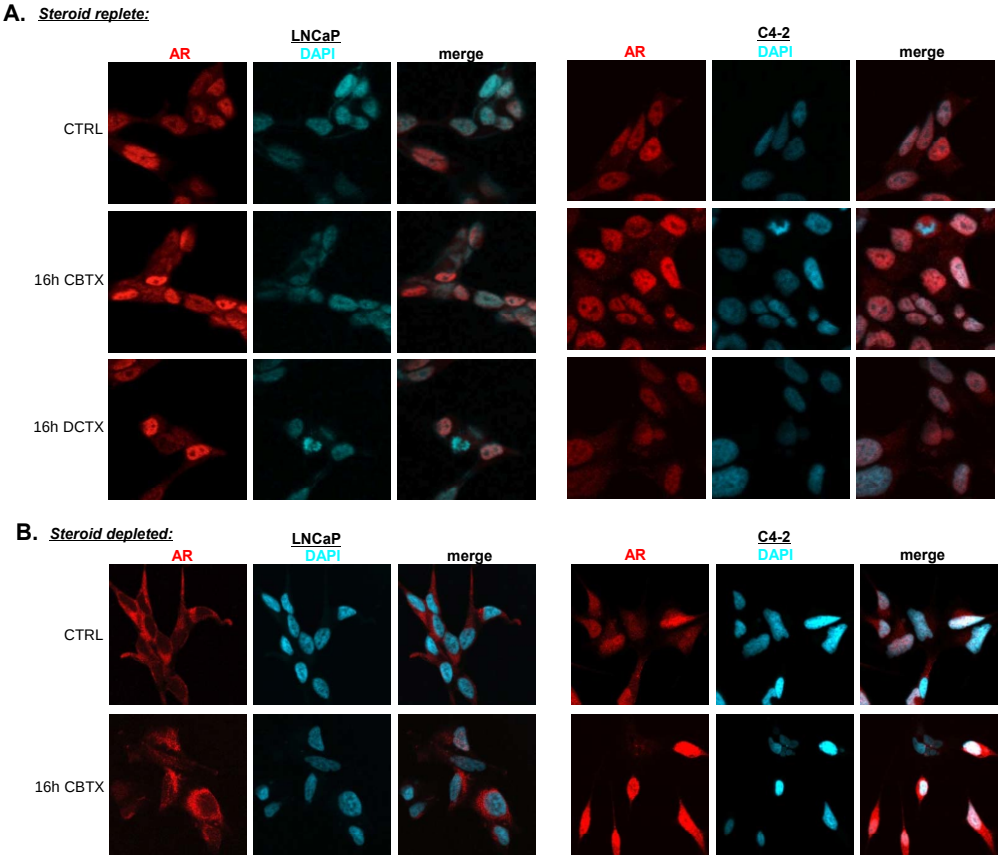

***Figure 3*: The effects of taxanes are independent of altered AR localization.** A. Immunofluorescence after 16h 1nM CBTX, DCTX or CTRL treatment demonstrates nuclear localization of AR (red) is unaffected in presence of steroids. DAPI staining (cyan) denotes cell nuclei. B. In androgen deprivation, AR resides in the cytoplasm of LNCaP cells, but remains nuclear in C4-2 CRPC cells in androgen deprivation conditions (-steroids), even after 16h cabazitaxel exposure.

Figure 4

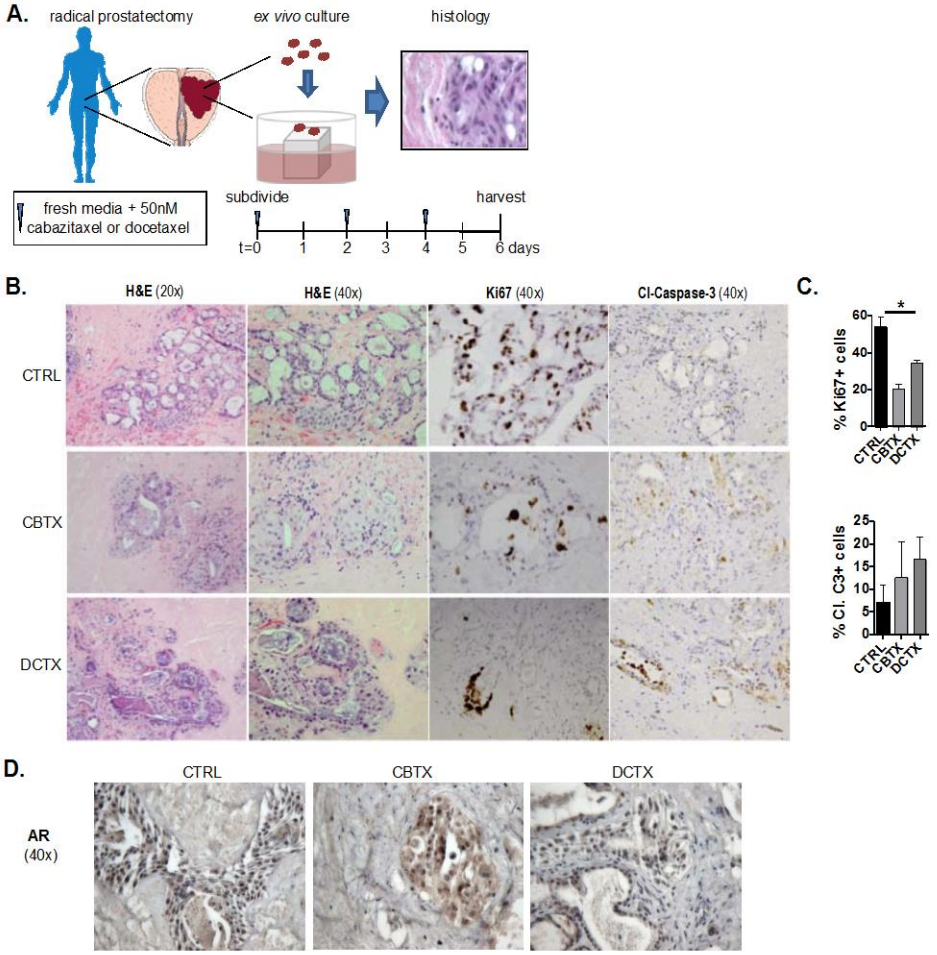

***Figure 4*: Cabazitaxel exerts enhanced anti-tumor effects in human tumors.** A. Schematic overview of the *ex vivo* explant assay. Fresh tissue obtained from radical prostatectomy is subdivided and cultured for 6 days on dental sponges submerged in cell culture media with different treatments (CTRL, 50nM CBTX or DCTX), after which tissue is formalin-fixed, paraffin-embedded, and analyzed by standardized immunohistochemistry (IHC) methods. B. H&E and IHC on explant tissues demonstrate that taxane treatment reduces tumor cell proliferation (Ki67) and induces cell death, (Caspase-3). C. Quantification of Ki67 (top) in three independent explant assays, performed on tissue from three patients, shows reduced proliferation in cabazitaxel treated samples compared to control ($p<0.05$ by Kruskal-Wallis non-parametric multiple comparison analysis). Cabazitaxel demonstrates improved drug efficacy compared to docetaxel *ex vivo*. Quantification of Caspase-3 in the three explant assays (bottom) indicates a moderate, yet non-significant increase in cell death, as induced by taxane treatment. D. AR (IHC) remains nuclear in tumor specimens after 6 days of taxane treatment.

Figure 5

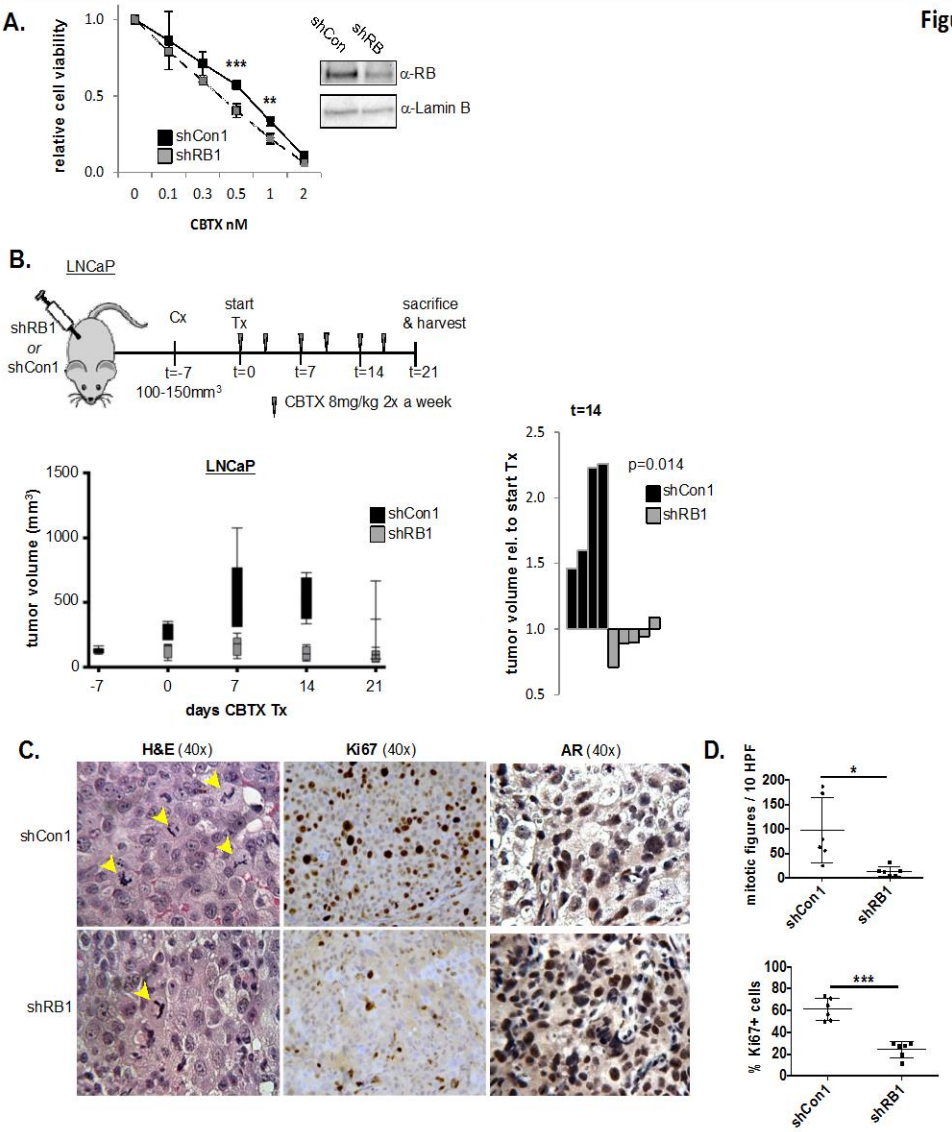

***Figure 5*: Tumors that progress to CRPC by RB loss show hypersensitivity to cabazitaxel.** A. RB knockdown LNCaP cells (shRB1) show a modest sensitization *in vitro* to 48h cabazitaxel and 96h in fresh media (no CBTX) in culture conditions mimicking androgen deprivation therapy (ADT), but not in presence of hormones (in serum), as measured cell viability in a trypan blue exclusion assay. B. Treatment schematic for nude athymic mice, subcutaneously injected with LNCaP shRB1 or LNCaP shCon1 cells to obtain xenograft tumors *in vivo* (n=5 per group). Growth analysis of xenograft tumors was monitored over time of CBTX treatment (start t=0). The graph on the right denotes the sizes for each tumor at t=14 relative to the size at start of treatment (t=0), showing that only LNCaP shRB1 tumors respond to CBTX (p=0.014). C. RB proficient LNCaP xenograft tumors display decreased Ki67 staining (unpaired ttest: p<0.0001), and elevated numbers of mitotic figures after CBTX treatment. AR remains nuclear after CBTX exposure, irrespective of RB status. D. Quantification of mitotic figures (top) and Ki67 positive cells (bottom) in 10 High Power Fields (HPF, 400x) per tumor show elevated % of mitotic figures in shCon1 tumors, and a reduction in proliferating cells in shRB1 tumors.

Figure 6

A.

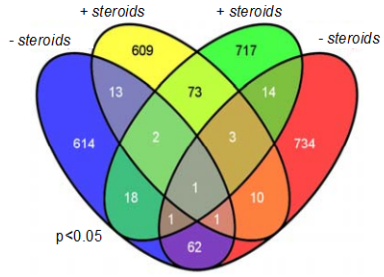

B. Top 25 hits

CBTX androgen deprived UP		CBTX androgen deprived DOWN	
gene	fold	gene	fold
LHX3	1.7749	STARD13	-1.59
RNLS	1.6769	RMI2	-1.523
CIDEC	1.623	ZMYND10	-1.496
RELT	1.6082	GPC6	-1.473
OR10C1	1.5813	RPS6KA5	-1.469
GGT5	1.5577	ORC6	-1.468
RUNX1	1.5233	TUBGCP5	-1.463
TMEM100	1.5073	NADSYN1	-1.439
PIM1	1.4997	AFAP1L2	-1.401
IL1RAP	1.4993	CXCL1	-1.396
PRDM8	1.4561	E2F7	-1.387
C4B	1.4557	RASSF8	-1.379
KCNH6	1.4473	AKR7A3	-1.373
CGB	1.4342	COX4I2	-1.369
AREG	1.4339	CDC6	-1.367
LRRC7	1.4338	RGP1	-1.36
CSN3	1.428	CD27	-1.346
KCNJ10	1.4051	ARL4D	-1.344
KCNC3	1.4046	ANGPTL7	-1.343
OR51M1	1.4034	CCDC88C	-1.34
HEPHL1	1.3979	RAB3IL1	-1.339
PRAMEF10	1.3977	GPR89C	-1.332
GAST	1.3915	KIF23	-1.327
DEFA1B	1.3888	OIP5	-1.324
SPEG	1.3887	ALDH16A1	-1.322

CBTX steroid replete UP		CBTX steroid replete DOWN	
gene	fold	gene	fold
NLRP13	1.81	TRAIP	-1.57
FERD3L	1.69	THSD4	-1.57
CAMKMT	1.66	OGN	-1.53
LGR6	1.65	ABCC3	-1.51
WNT3A	1.62	PTPDC1	-1.47
AP1M1	1.58	IGLJ5	-1.42
ZFAND6	1.57	FANCD2	-1.40
NAV3	1.51	ERG	-1.38
ANK2	1.51	TMCO7	-1.38
OBSL1	1.50	ALDH3A1	-1.38
IL28RA	1.50	MAPK10	-1.38
OR2AK2	1.48	LYZ	-1.36
SLC34A2	1.47	NFKBIZ	-1.35
BTLA	1.45	TIGD4	-1.35
TMEM88B	1.44	NOBOX	-1.34
WDR81	1.44	IL1A	-1.34
HTR2C	1.43	LHFP	-1.34
IFIT5	1.43	MDC1	-1.33
ECEL1	1.42	NOS1	-1.33
PNLIPRP3	1.41	ENTHD1	-1.33
TRIM15	1.40	CYP8B1	-1.32
FMOD	1.40	ZNF630	-1.31
PDZD3	1.39	SCGB2A2	-1.31
PNMA5	1.39	DNAH10	-1.31
NODAL	1.38	VAV1	-1.31

C. GO analysis (p<0.05)

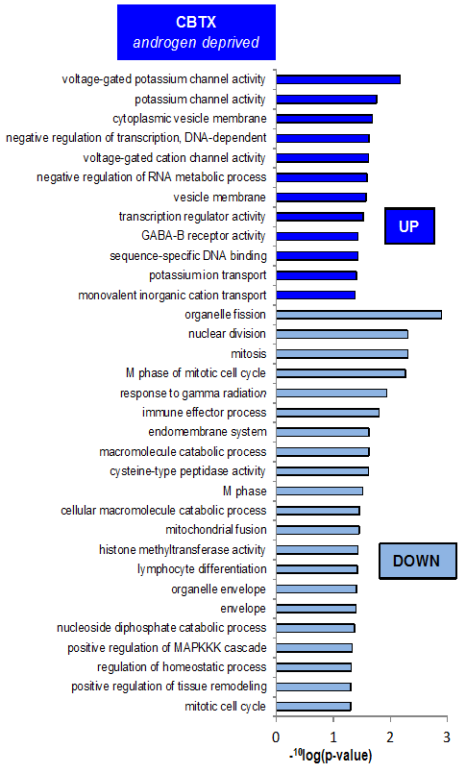

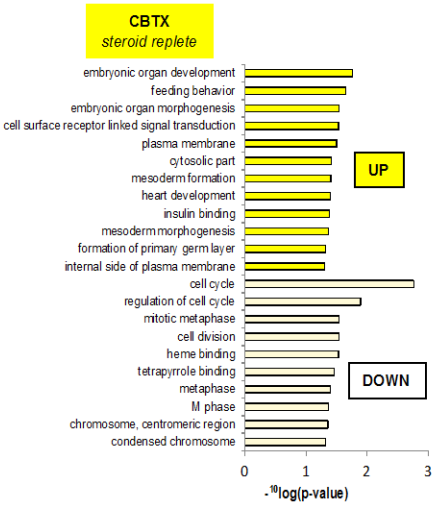

D. AR targets:

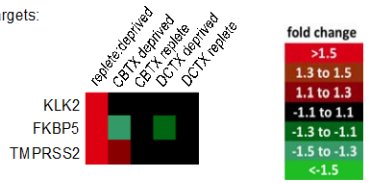

***Figure 6*: Expression profiling reveals novel action(s) of cabazitaxel in prostate cancer cells.** A. Venn diagram of a microarray analysis of p<0.05 after background filtering reveals differential response of castrate-sensitive LNCaP cells to 16hrs 1nM CBTX compared to DCTX, dependent on culture conditions: steroid rich (+) versus depleted (-) media, in triplicate. B. Top 25 significant hits of CBTX unique in androgen deprived (blue) or steroid replete (yellow) conditions are displayed with the corresponding mean fold change over control treated samples. C. David bioinformatics analysis of CBTX specific genes in castrate (blue, corresponding with Venn cluster) or steroid replete (yellow) displays GO-term enrichment of cell cycle genes, which confirms drug effects in mitosis. C. Heatmap of AR target genes: differential expression in steroid replete versus deprived (first column), and taxane versus control under different steroid conditions, as labeled.

Research Project 3: Project Title and Purpose

Increasing Colorectal Cancer (CRC) Screening in Primary Care among African Americans - Determine the impact of behavioral interventions on CRC screening, and the use of CRC screening tests among African American patients, in primary care practices 12 months after enrollment in the study.

Anticipated Duration of Project

1/1/2011 – 12/31/2014

Project Overview

This project will build on a current trial being conducted in primary care practices affiliated with Thomas Jefferson University (TJU) and the Albert Einstein Health Network (AEHN) in Philadelphia. A randomized, controlled study of behavioral interventions, intended to boost colorectal cancer (CRC) screening, assesses the status of patients six months after randomization. We will extend the screening observation period after random assignment from 6 to 12 months per patient. The additional time will allow for the complete ascertainment of CRC screening use and specific screening procedures (e.g., colonoscopy screening). In this project, we will also develop and pilot test new patient recruitment procedures. Patients will be able to register in their primary care practices to be contacted by study personnel, relative to enrollment. Furthermore, we will audio record patient navigation telephone calls for analysis. The analyses will seek to identify barriers to and facilitators of successful navigation. Focus groups will be conducted with study participants who screened (one group for women and one group for men), and those who did not screen (one group for women and one group for men), within the 12-month observation period. Two additional focus groups (one with Hispanic men and one with Hispanic women who are patients in AEHN practices) will also be conducted. These focus groups will be conducted to learn what factors influenced response to intervention. Patient-related screening costs, and information on insurer payments related to increases in CRC screening rates will be analyzed. Finally, we will translate intervention materials into Spanish to broaden the reach of intervention contacts. Results of these analyses will support the design of an enhanced CRC screening intervention system.

Principal Investigator

Ronald E. Myers, PhD
Professor and Director
Department of Medical Oncology
Thomas Jefferson University
1015 Walnut Street, Suite 1014
Philadelphia, PA 19107

Other Participating Researchers

Randa Sifri, MD – employed by Thomas Jefferson University

Expected Research Outcomes and Benefits

The project will provide measures of CRC screening, and the use of specific screening tests, within 12 months after intervention. Additional analyses will be performed to determine important mediators and moderators of CRC screening among study participants; develop effective patient recruitment strategies, and identify barriers to and facilitators of response to CRC screening interventions in population subgroups. Findings from these analyses, along with results of patient-specific cost analyses will help to inform the development of an improved CRC screening navigation system for use in primary care. The project will also result in the production of CRC screening intervention materials for use with Hispanic patients.

Summary of Research Completed

Mediators and Moderators of CRC Screening

In this analysis, we attempted to identify mediating variables, which are defined as variables that are in the causal pathway between intervention and screening. We investigated a global Preventive Health Model (PHM) measure as well as its five subscales, as potential mediators. However, we found that baseline-to-endpoint changes in these six measures were small, and did not differ significantly between the Tailored Navigation Intervention (TNI) and Standard Intervention (SI) groups (Table 1). Therefore, we conclude that differences in screening rates between the study groups are not due to the study groups' differential impact on the PHM scales.

In terms of moderator analyses, Table 2 displays results concerning interactions between study group and several participant attributes on 12 month screening. Here we present the odds ratio for TNI vs SI within the levels of the potential moderator variables. None of the predictor variables showed a significant interaction.

Additional analyses, (not shown in Table 2), were conducted on the five PHM subscales. For the global PHM score as well as the individual PHM subscales, the contrast between TNI and SI was somewhat stronger among participants with less favorable attitudes toward screening (low susceptibility, low salience, low response efficacy, high worries, low social support and influence). The only subscale that had an appreciable impact on the relationship between the intervention and screening was response efficacy. At 12 months the effect of TNI vs. SI was greater for participants with lower response efficacy (OR = 3.91) than those with higher response efficacy (OR = 1.51). Thus, TNI tended to have a greater, marginally significant (p=0.06) effect among those with lower response efficacy, than those with higher response efficacy.

Identification of Barriers and Facilitators to Screening

Data collection on barriers and facilitators of CRC screening occurred during the endpoint survey. An endpoint telephone survey was administered to 519 participants (68%). Of these, we were able to gather data screening barriers from 243 participants who did not complete screening and screening facilitators on 125 participants who did complete screening. Participants were asked to report a primary reason for their adherence or non-adherence to CRC screening, respectively. The data were qualitatively analyzed to identify types of screening barriers and facilitators.

Of the 243 participants who reported screening barriers, we found that the primary reasons for non-adherence were distributed as follows: low perceived importance of CRC screening (28%), lack of transportation or time needed to attend a screening appointment (17%), fear of screening or results (11%), dislike of screening procedures (11%), lack of insurance coverage or limited capacity to pay for screening and follow-up (10%), confusion about the screening process (10%), existence of a health condition that precluded screening (8%), and other reasons (5%).

Of the 125 participants who reported screening facilitators, we found that the primary reasons for adherence were distributed as follows: high perceived importance (30%), awareness of a known risk factor, such as age or race (30%), social support/doctor recommendation (24%), study contact (12%), convenience of screening (2%) and insurance coverage (1%).

Cost Analysis

In order to examine the cost effectiveness of the TNI versus SI, overall cost was divided among participants and per person cost will be compared. Overall cost divided among participants was reported previously. Currently, data for per person cost is being analyzed. Per person cost accounts for both fixed and differentiated costs for each enrolled participant. Data points include, but are not limited to, the cost of introduction mailing and completion of the baseline telephone call, mailing of intervention materials and completion of navigation. Data sources currently being entered and reviewed are staff time logs, study invoices, participant call logs, the study tracking database and the current market price of supplies. Personnel costs for each activity have been divided among the intervention arms by number of patients in each group and number of patients involved in each activity, while supplies for each participant have been individually determined. Activity cost/completion differs based on study arm and the active participation of the patient.

The baseline survey cost is estimated at 33 percent of recorded time, eliminating time required for research and including time to introduce the study, assess eligibility and for asking questions about test preference. Where baseline survey time is missing, 33 percent of the average will be applied. Baseline survey cost will only be included for the TNI Group, which required eliciting preference to condition a preference-based mailing. SI Group participants received a generic mailing that could be sent to members of a practice without a baseline survey.

Personnel costs are computed by time of each activity (assembling mailings, completing navigation calls etc.) by adjusted salary per minute, using the base salary for each position to calculate the adjusted salary per minute**.** Activity costs were determined using staff time logs and recorded start and end times of telephone calls. Supplies include questionnaires, printing costs, envelopes, paper, postage, cell phone use and other resources used to enroll participants and produce intervention materials. Costs were calculated by quantifying the materials for each activity and pricing according to current market rates. Professionally printed materials were accounted from project invoices.

Tables

Table 1. Baseline-to-endpoint change in PHM scales (N = 517).*

	SI	**TNI**	**TNI vs. SI**	
	mean (sd)	*mean (sd)*	*mean diff (95% CI)*	*P*
Global PHM scale				
Baseline	3.9 (0.6)	3.9 (0.5)		
Endpoint	3.8 (0.6)	3.8 (0.6)		
Baseline-to-endpoint change	-0.1 (0.6)	0.0 (0.5)	0.0 (-0.1, 0.1)	0.489
Perceived susceptibility				
Baseline	2.6 (1.1)	2.5 (1.1)		
Endpoint	2.5 (1.2)	2.5 (1.2)		
Baseline-to-endpoint change	-0.1 (1.3)	0.0 (1.2)	0.1 (-0.1, 0.2)	0.580
Screening salience				
Baseline	4.8 (0.5)	4.8 (0.5)		
Endpoint	4.8 (0.5)	4.9 (0.4)		
Baseline-to-endpoint change	0.0 (0.5)	0.0 (0.6)	0.1 (0.0, 0.1)	0.088
Screening response efficacy				
Baseline	4.4 (0.8)	4.5 (0.7)		
Endpoint	4.6 (0.8)	4.5 (0.8)		
Baseline-to-endpoint change	0.1 (0.9)	0.0 (0.8)	0.0 (-0.1, 0.1)	0.943
Worries and concerns				
Baseline	3.0 (1.4)	2.8 (1.4)		
Endpoint	2.7 (1.4)	2.6 (1.4)		
Baseline-to-endpoint change	-0.3 (1.4)	-0.2 (1.4)	-0.1 (-0.3, 0.2)	0.602
Social support and influence				
Baseline	4.2 (0.9)	4.3 (0.8)		
Endpoint	4.2 (0.8)	4.2 (0.8)		
Baseline-to-endpoint change	-0.1 (0.9)	-0.1 (0.9)	0.0 (-0.1, 0.2)	0.469
Religiosity/fatalism				
Baseline	2.5 (1.1)	2.5 (1.0)		
Endpoint	2.5 (1.1)	2.5 (1.1)		
Baseline-to-endpoint change	0.0 (1.1)	0.0 (1.0)	0.0 (-0.2, 0.2)	0.902

Mean diff: mean difference (adjusted for study wave and practice, participant age, sex, education, marital status, baseline decision stage, baseline preferred test, and the baseline value of each outcome). CI: confidence interval.

(*) N = 517 for global PHM scale, 499 for susceptibility, 516 for salience, 485 for response efficacy, 499 for worries and concerns, 504 for social support and influence, and 488 for religiosity/fatalism.

Table 2. Effects of the intervention (TNI versus SI) on CRC screening at 12 months, within categories of various participant characteristics.

	Screening (%)		**TNI vs SI**		
	SI	*TNI*	*OR*	*(95% CI)*	*Interaction P-value*
Age x Study group					0.405
50-59	29%	40%	1.53	(1.05, 2.22)	
60+	38%	55%	2.05	(1.15, 3.66)	
Sex x Study group					0.533
Female	34%	46%	1.78	(1.23, 2.58)	
Male	29%	37%	1.43	(0.80, 2.54)	
Education x Study group					0.548
High school or less	31%	40%	1.54	(1.02, 2.32)	
Greater than high school	34%	48%	1.87	(1.15, 3.02)	
Marital status x Study group					0.310
Married (or living as married)	37%	45%	1.32	(0.76, 2.29)	
Single/divorced/widowed	30%	43%	1.86	(1.28, 2.73)	
Global PHM scale x Study group					0.507
Low (1.0-3.0)	30%	48%	2.43	(0.77, 7.73)	
High (3.1-5.0)	32%	43%	1.62	(1.17, 2.24)	
Screening decision stage x Study group					0.547
Decided against to undecided	16%	31%	2.30	(0.77, 6.80)	
Decided to do	34%	45%	1.62	(1.17, 2.24)	
Preferred screening test x Study group					0.344
Stool blood test	30%	53%	1.48	(0.98, 2.24)	
Equal preference	33%	41%	2.77	(1.31, 5.87)	
Colonoscopy	31%	42%	1.53	(0.82, 2.86)	

OR: adjusted odds ratio for TNI versus SI (simultaneously adjusted for all variables shown plus study wave and practice). CI: confidence interval.

Research Project 4: Project Title and Purpose

Targeting Endoplasmic Reticulum Stress (ERS) Signaling for Overcoming Lung Cancer Resistance - Lung cancer patients die as a consequence of therapeutic resistance and treatment failure. One of the important features of cancer resistance is the inability to undergo apoptosis. Ongoing research from this laboratory supports the idea of inducing ER stress-mediated autophagy as a way of combating resistant lung cancer cells. Therefore we will investigate the underlying mechanisms and preclinical concepts of using ER stress activators for enhancing radiotherapy in treating lung cancer.

Anticipated Duration of Project

1/1/2011 - 12/31/2014

Project Overview

Tumor cells, as a result of transformation or tumor microenvironment, have dysregulated signaling pathways that control cell survival or death. This enables the cells to evade programmed cell death (apoptosis) following treatment with cancer therapies. In every tumor, there is a population of cells that harbors multiple genetic defects in a major form of apoptosis. These cells are enriched following cytotoxic chemotherapy such as cisplatin and become a source of failure due to therapeutic resistance. This laboratory has identified an alternative death program, autophagy (self-eating), which can be triggered in cells that are defective in apoptotic signaling and that overcome tumor resistance to ionizing radiation (IR). The translational potential of this concept uses model systems of several chemical agents that increase IR-induced cell death, even in the presence of defective apoptotic machinery. In these systems, the radio-sensitizing mechanism is dependent upon autophagy mediated by PERK-dependent endoplasmic reticulum stress (ERS) signaling. This project will extend this work using *in vitro* and *in vivo* cancer models, and lung cancer cell clones that are resistant to cisplatin and IR.

The hypothesis is that in tumor cells lacking functionally intact apoptosis, ERS regulates the IR response through autophagic pathways. To validate this theory, both cancer cells with known apoptotic gene defects and cancer cells fully resistant to cisplatin will be used to determine the key molecules that regulate ERS and autophagy signaling. The following four aims are proposed:

(1) Determine if the regulation of ERS is a significant molecular target of the cellular damage response that occurs during IR-induced autophagy;
(2) Determine the mechanism by which caspases 3/7 regulate ERS signaling in the IR response;
(3) Determine whether ERS inducers increase IR sensitivity in *in vitro* cancer models;
(4) Determine whether ERS inducers increase IR sensitivity in *in vivo* cancer models.

Principal Investigator

Adam P. Dicker, MD, PhD
Professor and Chair
Department of Radiation Oncology
Thomas Jefferson University
111 South 11th Street
Philadelphia, PA19107

Other Participating Researchers

Bo Lu, MD, PhD – employed by Thomas Jefferson University

Expected Research Outcomes and Benefits

Cancer mortality is due to ineffective cancer therapies. Lung cancer alone is responsible for more deaths than most other cancers combined and remains a huge challenge to the general public, treating physicians and our health care system. While prevention and early detection are important, the vast majority of lung cancer patients will present with advanced, incurable disease requiring systemic medical therapy and local regional radiotherapy. The unfortunate fact is that most of these treatments will fail, presumably owing to the intrinsic resistance of tumor cells to apoptotic cell death. This project will *to determine whether ERS signaling is regulated by molecules that orchestrate apoptotic cell death, and whether ERS can be targeted to induce alternative programmed cell death, i.e., autophagic cell death*. This concept will be tested in cisplatin-resistant lung cancer cells, which, owing to their extreme resistance to apoptosis, are the potential source of recurrence of locally advanced lung cancer after treatment with chemoradiation. The hope is that this research strategy will eventually improve the outcomes of lung cancer patients.

The overarching theme of this research is that, when apoptosis is dysfunctional, IR–induced cell death is mediated by PERK-dependent ERS signaling. This project will test the novel idea that downstream pro-apoptotic molecules (caspases) regulate ERS signaling, triggering an alternative cell death program (autophagy). The feasibility of targeting ERS will be tested to sensitize lung cancer cells that are resistant to cisplatin and IR. Using these novel lung cancer cell models, we will identify the associated molecular biomarkers and define methods to overcome therapy resistance.

Summary of Research Completed

We previously reported that IGFBP-3 was significantly down regulated in cisplatin-resistant lung cancer cells, making it a molecule of interest in exploring treatment-induced lung cancer resistance.

<u>Overexpression of IGFBP-3 inhibits survival in HCC2429 cells</u>

To study the effect of IGFBP-3 on the survival of two lung cancer cell lines (HCC2429 cells and H460 cells), we used adenoviral vector to overexpress IGFBP3. Ad-IGFBP-3 and its control virus, Ad-EV were used to infect these lung cancer cells. Western analyses demonstrated that IGFBP-3 was highly expressed 72h after infection in both HCC2429 cells and H460 cells as shown in Figure 1A. To determine the impact of IGFBP3 expression on cell survival, MTS assay was performed 72 h after exposing lung cancer cells with the IGFBP-3-expressing adenovirus. Survival of HCC2429 cells was reduced to half while only 10% of survival reduction was detected in H460 cells (Figure 1B).

<u>IGFBP-3 inhibits cell survival partially through blocking IGF-1 signaling</u>

IGFBP-3 binds to IGF-1 and prevents IGF-1 to activate IGF-1R and its downstream signaling. In order to determine whether IGFBP-3 inhibition of cell survival is dependent upon its interaction with IGF-1, we used IGFBP-3 ^{GGG} mutant, which has no binding affinity to IGF-1 (Figure 2A).

72 h after HCC2429 cells were exposed to Ad-IGFBP-3 infection, we observed 40% survival reduction in HCC2429 whereas only 20% survival reduction was seen following the exposure of Ad- IGFBP-3 ^{GGG}. In contrast, neither virus affected survival of H460 lung cancer cells.

IGFBP-3 inhibits cell survival partially through blocking IGF1 signaling. Figure 2a, schematic structure of IGFBP-3 and its mutant, IGFBP-3^{GGG}; Figure 2b, HCC2429 and H460 cells were infected with Ad-IGFBP-3, Ad-IGFBP-3 mutant and Ad-EV. MTS assay was performed 72 h after infection; Figure 2c, HCC2429 and H460 cells were infected with Ad-IGFBP-3, Ad-IGFBP-3 mutant and Ad-EV, 72h post infection, cells were collected and protein samples were extracted. Various signaling proteins were probed. As shown in Figure 2c, baseline signaling is different in the two cell lines. HCC2429 cell showed active phosphorylated IGF-1R and Akt but no active STAT3, in contrast to H460 cells. Both cell models have high level of phosphorylated ERK. When IGFBP-3 is overexpressed, active IGF-1R and ERK were suppressed in HCC2429 cells. Neither alteration was seen in the H460 cell line. Overexpression of the non IGF-1-binding mutant partially decreased ERK phosphorylation in HCC2429 cells.

Overexpression of IGFBP-3 increases susceptibility to cisplatin treatment in lung cancer cells

Since IGFBP-3 inhibits lung cancer cell survival and is reduced in cisplatin-resistant lung cancer cells in our previous study, we further explore its potential to enhance the efficacy of cisplatin chemotherapy. HCC2429 cell survival is decreased to 60% by either cisplatin treatment or IGFBP-3 overexpression whereas either treatment decreased H460 cell survival by ~40% and ~20% respectively as shown in Figure 3a. For H460 cells, the survival reduction was associated with a decrease in STAT3 phosphorylation (CDDP and IGFBP-3 OE) and a decrease in Akt phosphorylation (CDDP). For HCC2429 cells, we observed decreased IGF1R phosphorylation and STAT3 expression following IGFBP-3 overexpression, and Akt phosphorylation following CDDP or IGFBP-3 OE. Changes in ERK phosphorylation were: 1). An increase after CDDP treatment, 2). A decrease after IGFBP-3 OE as shown in Figure 3b. Combining IGFBP3 and CDDP decreased survival of HCC2429 by 80% and by 45% in the setting of H460. In H460 cells, the combined treatment abrogated STAT3 phosphorylation and decreased Akt phosphorylation. In HCC2429 cells, STAT3 expression, Akt phosphorylation and ERK phosphorylation were greatly attenuated.

48h after treatment, caspase-3 cleavage was noted in H460 cells treated with either CDDP or IGFBP-3 overexpression and became more pronounced after the combined treatment as shown in Figure 3c. CDDP-treated HCC2429 cells showed significant increases in caspase-3 cleavage, whereas IGFBP-3 overexpression has a mild effect. Combination treatment resulted in a significant increase of caspase-3 cleavage.

IGFBP-3-overexpression induces ER stress and IGFBP-3-induced apoptosis is dependent on GRP78

We hypothesized that the observed therapeutic efficacy of IGFBP3 is mediated by ER stress signaling.
Therefore, ER stress markers, GRP78 and phospho-eIf2a, were probed and found to be induced 48h following Ad-IGFBP-3 infection in both HCC2429 and H460 cells as shown in Figure 4A.

We then used GRP78 siRNA to determine whether GRP78 is responsible for IGFBP-3 induced apoptosis. As shown in Figure 4B, GRP78 knockdown attenuated IGFBP-3 induced apoptosis in HCC2429 cells.

IGFBP-3-overexpression induces ER stress and IGFBP-3-induced apoptosis is dependent on GRP78. Figure 4a, HCC2429 and H460 cells were infected with Ad-IGFBP-3, Ad-IGFBP-3 mutant and Ad-EV, Cells were collected and protein was extracted for immunoblotting; Figure 4b, HCC2429 and H460 cells were transfected with GRP78 siRNA or a control siRNA. 24 h after transfection, cells were infected with either Ad-IGFBP-3 or Ad-EV. Cells were collected 72 h later. Protein was extracted for immunoplotting of GRP78, IGFBP-3 or caspase 3.

Fig 1A

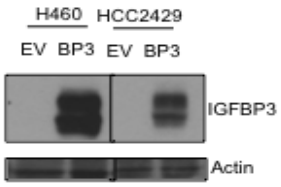

Fig 1B

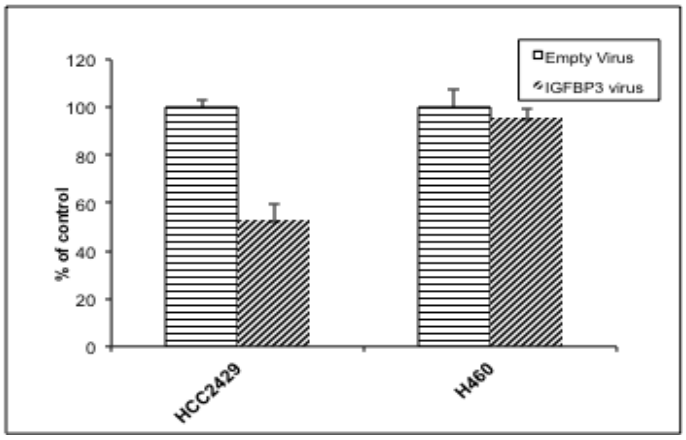

Figure 1: Overexpression of IGFBP-3 inhibits survival of HCC2429 cells. Figure 1a, HCC2429 and H460 cells were infected with Ad-IGFBP-3 or a control virus, Ad-EV. 72 h later, cells were collected and protein was extracted, immunobloting was performed using IGFBP-3 antibody. Figure 2b, HCC2429 and H460 cells were infected with Ad-IGFBP-3 or Ad-EV, MTS survival assay was performed 72 h after infection.

Fig 2A

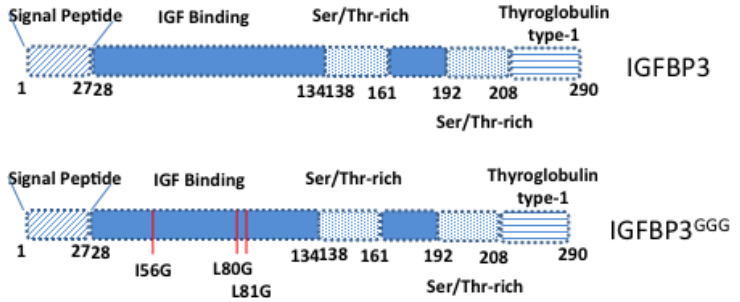

Fig 2B

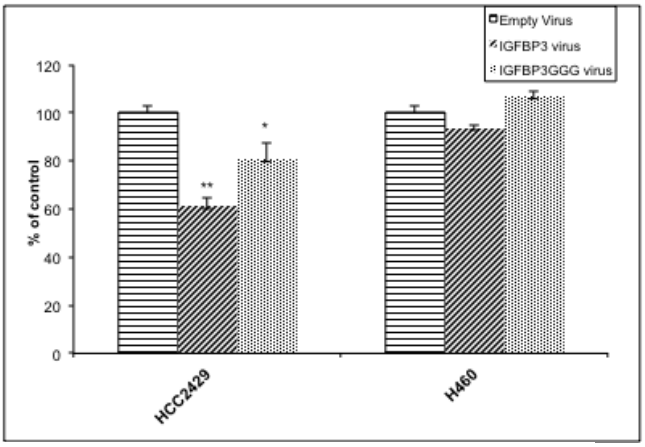

Fig 2C

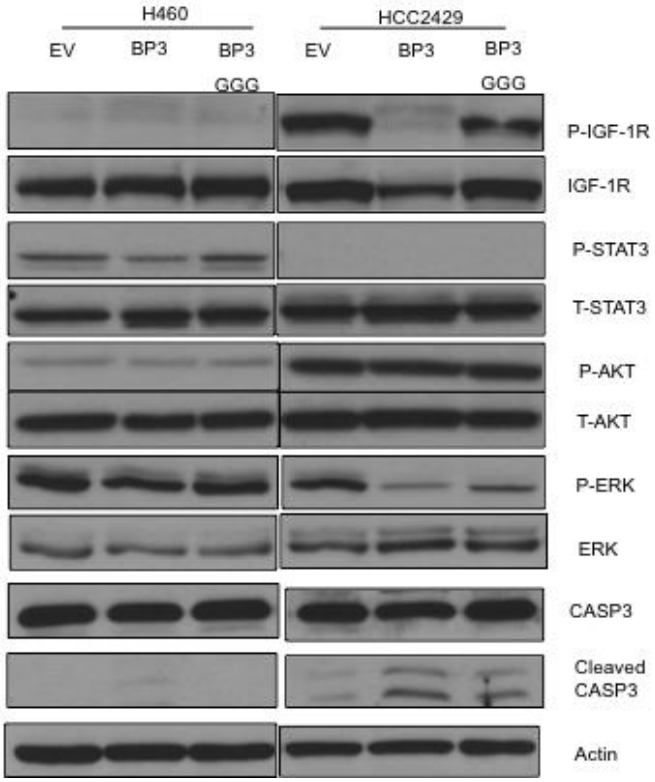

Figure 2: IGFBP-3 inhibits cell survival partially through blocking IGF1 signaling. Figure 2a, schematic structure of IGFBP-3 and its mutant, IGFBP-3^{GGG}; Figure 2b, HCC2429 and H460 cells were infected with Ad-IGFBP-3, Ad-IGFBP-3 mutant and Ad-EV. MTS assay was performed 72 hours after infection; Figure 2c, HCC2429 and H460 cells were infected with Ad-IGFBP-3, Ad-IGFBP-3 mutant and Ad-EV, 72hr post infection, cells were collected and protein samples were extracted. Various signaling proteins were probed. As shown in Figure 2c, baseline signaling is different in the two cell lines. HCC2429 cell showed active phosphorylated IGF-1R and Akt but no active STAT3, in contrast to H460 cells. Both cell models have high level of phosphorylated ERK. When IGFBP-3 is overexpressed, active IGF-1R and ERK were suppressed in HCC2429 cells. Neither alteration was seen in the H460 cell line. Overexpression of the non IGF-1-binding mutant partially decreased ERK phosphorylation in HCC2429 cells.

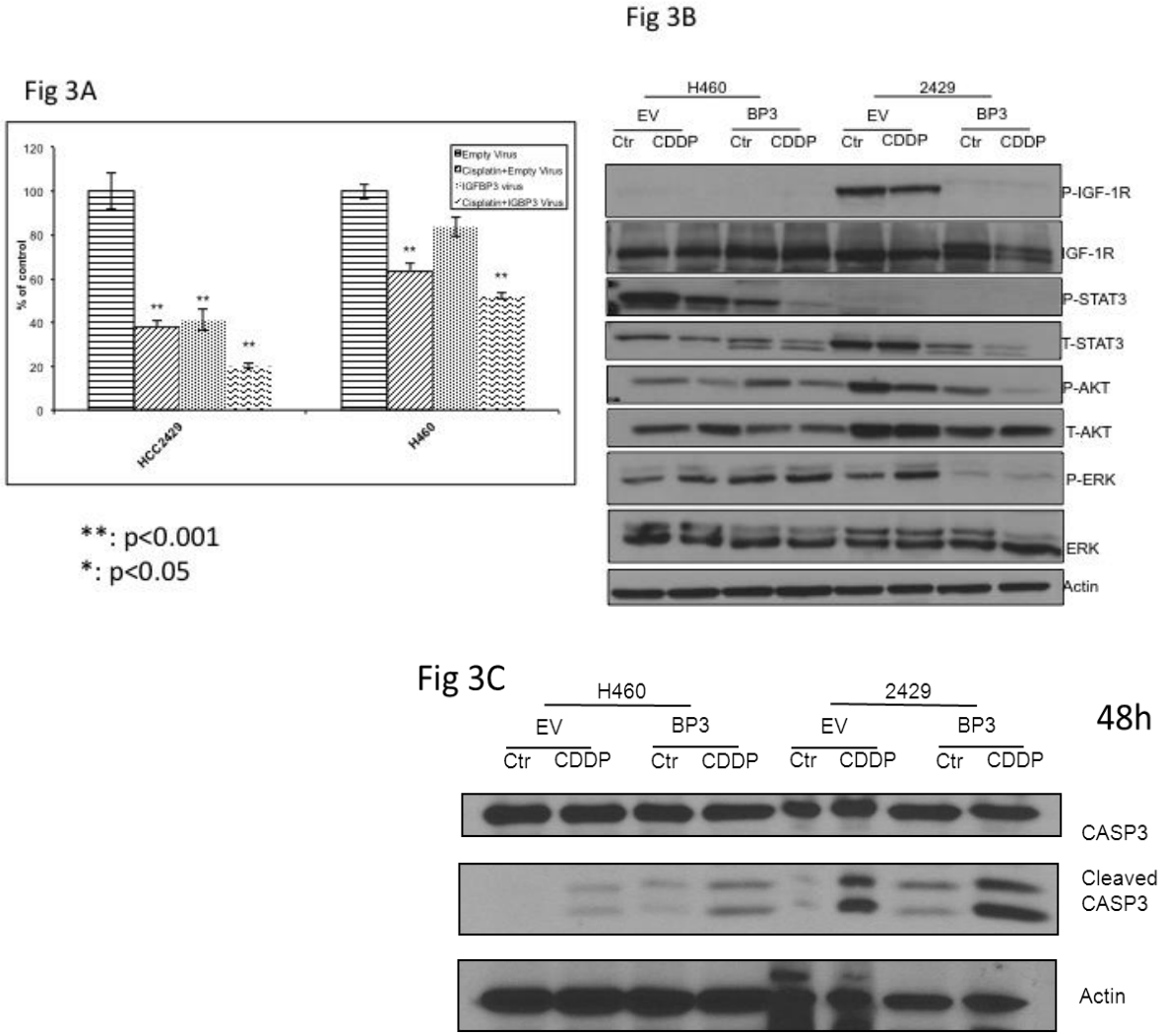

Figure 3: Overexpression of IGFBP-3 increases susceptibility to cisplatin treatment in lung cancer cells. Figure 3a, HCC2429 and H460 cells were infected with Ad-IGFBP-3, and Ad-EV, 72 hr post infection, cells were treated with 20 µM cisplatin. MTS assay was performed 24 hr after incubation, Figure 3b, HCC2429 and H460 cells were infected with Ad-IGFBP-3, and Ad-EV, 72 hr post infection, cells were treated with 20 µM cisplatin. Cells were collected for protein extraction and immunoblotting.

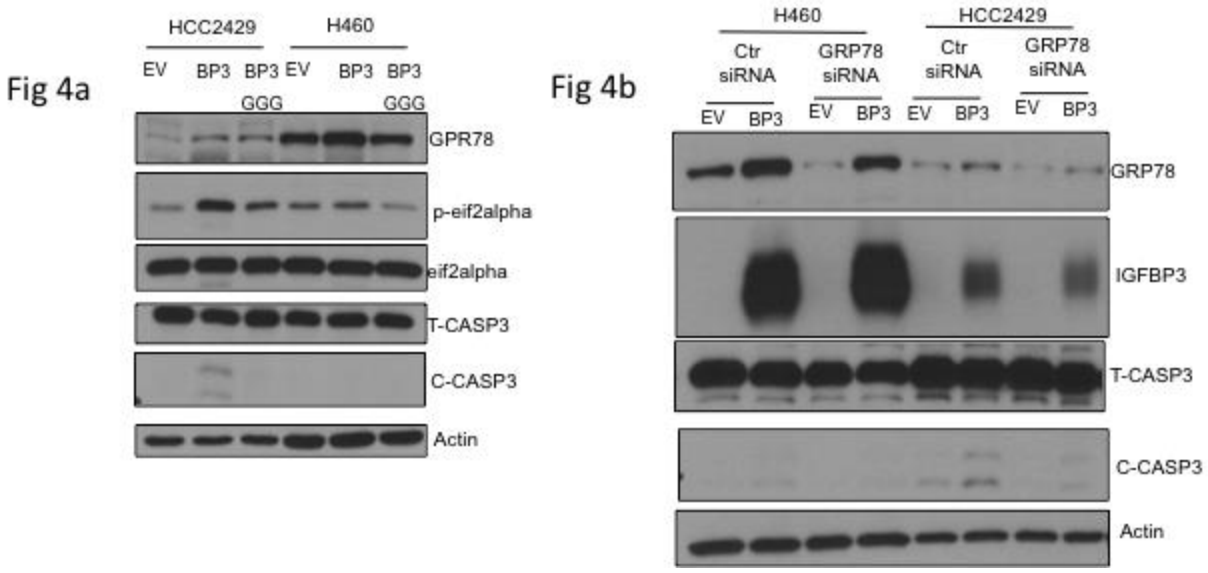

Figure 4: IGFBP-3-overexpression induces ER stress and IGFBP-3-induced apoptosis is dependent on GRP78. Figure 4a, HCC2429 and H460 cells were infected with Ad-IGFBP-3, Ad-IGFBP-3 mutant and Ad-EV, Cells were collected and protein was extracted for immunoblotting, Figure 4b, HCC2429 and H460 cells were transfected with GRP78 siRNA or a control siRNA. 24 hrs after transfection, cells were infected with either Ad-IGFBP-3 or Ad-EV. Cells were collected 72 hrs later. Protein was extracted for immunoplotting of GRP78, IGFBP-3 or caspase 3.

Research Project 5: Project Title and Purpose

New Stem/Progenitor Cell-Related Biomarker(s) for Predicting DCIS Prognosis and Progression - Ductal Carcinoma *In Situ* (DCIS) is characterized by a clonal proliferation of malignant epithelial cells confined within the lumens of mammary ducts, without invasion into adjacent stroma. Since DCIS represents a group of biologically and morphologically heterogeneous diseases, its classification and management remains very challenging. Breast conserving therapy with or without radiotherapy is the accepted treatment for most cases of DCIS. However, the local recurrence rate with such therapy ranges from 10 to 40% with half of these patients developing invasive carcinoma. Previous studies have attempted to identify prognostic molecular markers. Many of the molecules thought to play critical roles in progression of invasive breast cancer have not been shown to be independent prognostic markers for local recurrence or progression of DCIS. Therefore, there is a critical need to identify novel predictors of DCIS progression and potential targets for therapy.

Duration of Project

1/1/2011 - 9/01/2012

Summary of Research Completed

This project ended during a prior state fiscal year. For additional information, please refer to the Commonwealth Universal Research Enhancement C.U.R.E. Annual Reports on the Department's

Tobacco Settlement/Act 77 web page at http://www.health.state.pa.us/cure.

Research Project 6: Project Title and Purpose

Phenotypic and Molecular Characterization of Occult AML - The high incidence of relapse in acute myelogenous leukemia (AML) observed after induction of complete remission (CR) is thought to be due to the persistence in a protective niche in the bone marrow (BM). The residual AML cryptic cells are a rare population with self-renewal potential, representing Minimum Residual Leukemic Myeloblasts (MRLM). Homing of these AML cells in the BM is largely mediated through the interaction of the chemokine receptor CXCR4 expressed by AML cells with its ligand CXCL12 expressed by BM stromal cells. The objective of this project is to establish a rationale for mobilization of AML occult cells from the BM by treating patients in CR with a CXCR4 antagonist and demonstrating that AML precursor cells will be detected in bone marrow and peripheral blood as early predictor or relapse using cytogenics, multiparameter flow cytometry and next generation DNA sequencing.

Anticipated Duration of Project

1/1/2011 - 12/31/2014

Project Overview

The overall hypothesis of this proposal is that inhibition of CXCR4 could induce mobilization into peripheral blood of AML stem cells (AML-SC) hosted in the BM that constitute minimal residual disease during hematologic remission in patients with AML following stem cell transplantation (SCT). The objective of this project is to establish CXCR4 as a target for mobilization of AML occult cells in patients in CR after chemotherapy and allogeneic SCT and to establish the phenotypic and molecular signature of these AML myeloblats and AML-SC. Bone marrow and peripheral blood samples will be collected in a longitudinal study at 28, 90 and 180 days following SCT.

In Specific Aim 1, the identification of (recipient) leukemic myeloblasts will be performed using routinely performed techniques, including morphologic analysis and detection of cytogenetic abnormalities present at the time of the initial diagnosis and/or sex chromosome conversion following SCT using fluorescence *in situ* hybridization (FISH).

In Specific Aim 2, the identification and quantification of leukemic myeloblasts will be achieved by multiparameter flow cytometric detection of the abnormal phenotype present at the time of diagnosis using a panel of antibodies specific for myeloid markers and non-myeloid differentiation markers, as well as antigens associated with AML-SC such as CD34, CD117 (c-kit), CD123 (IL-3R alpha chain), CD47, and CXCR4.

In Specific Aim 3, the quantification of leukemic myeloblasts will be based on the analysis of hematopoietic chimerism using molecular genetic analysis of short tandem repeats (STR) alleles from donor and recipient genotypes. This will be achieved with the PowerPlex 16 assay routinely used to monitor chimerism following SCT. This assay consists of a set of multiplex PCR

amplification reactions and analysis of the length of the DNA fragments will be performed on an ABI3130 Genetic Analyzer. However, this traditional method offers a limited sensitivity due to the limited threshold of detection of traditional sequencers. The sensitivity of detection and the accuracy of quantification of chimerism will be extended by using next generation sequencing (Roche 454) to analyze the products of the PowerPlex 16 assay.

These specific aims will provide the tools to address the question as to whether mobilizing AML cells into peripheral blood and thereby sampling the entire marrow organ would be a reasonable strategy to detect residual or recurrent AML at an earlier time point than conventional marrow analysis.

Principal Investigator

Stephen C. Peiper, MD
Peter A. Herbut Professor and Chair
Jefferson Medical College of Thomas Jefferson University
1020 Locust Street
Philadelphia, PA 19107

Other Participating Researchers

Jean-Marc Navenot, PhD ; Neal Flomenberg, MD; Bing-hua Jiang, PhD; Ling-Zhi Liu, MD, PhD – employed by Thomas Jefferson University

Expected Research Outcomes and Benefits

Acute myelogenous leukemia (AML) is a heterogeneous disease, both phenotypically and at a genomic level. Although chemotherapy is frequently capable of achieving complete remission (CR), most adults with AML will relapse, even after allogeneic hematopoietic stem cell transplantation (SCT). It is widely accepted that relapse is due to the persistence in the bone marrow (BM) of a rare population of AML cryptic cells with self-renewal potential representing Minimum Residual Leukemic Myeloblasts (MRLM). These AML stem cells (AML-SC) have the capacity to initiate leukemia when transplanted in immune deficient mice and share functional and phenotypic features with normal hematopoietic stem cells (HSC). The expression of the chemokine receptor CXCR4 by AML-SC and of its ligand SDF-1/CXCL12 by BM stromal cells is responsible for their homing into a BM niche that protects them from obliteration by chemotherapy.

CXCR4 antagonism by blocking antibodies or by the small molecule antagonist plerixafor was shown in mouse models to prevent homing of AML-SC to the BM, to induce their mobilization into peripheral blood and to sensitize AML cells to chemotherapy, thus identifying CXCR4 as a potential target for the eradication of minimum residual disease (MRD) in AML. This project will use highly sensitive methods to establish the phenotypic and molecular signature of AML occult cells and will build a foundation for the future use of CXCR4 as a target for mobilization of AML-SC from the BM in patients with impending relapse of AML. The capacity to mobilize residual myeloblasts and AML-SC in peripheral blood would provide an early and more reliable

detection of residual or recurring leukemia compared to conventional BM sampling by effectively investigating the entire BM organ, thus allowing a better prediction of relapse and possibly improving the efficacy of therapeutic intervention.

Summary of Research Completed

From its inception, this project has focused on an important mechanism in tumor cell biology that has a critical impact on the clinical course of patients with malignant diseases: the ability of stromal cells to form a supportive niche to maintain rare, occult tumor cells during intervals of clinical remission. This model has been well established in patients with acute leukemia. It has been recognized for almost 50 years that a reservoir of undetectable leukemic blasts persist during intervals of clinical remission, characterized by normal hematopoiesis. In the absence of continued therapy, so-called maintenance therapy, patients invariable experience a relapse. Our initial goals were to use next generation sequencing to quantify minimal residual leukemic blasts during hematologic remission in patients with acute myelogenous leukemia (AML). There is evidence that the chemokines secreted by stromal cells plays a major role in the interaction of these cells with leukemic blasts that express the corresponding receptor(s). It has been postulated that this population contains/is composed of tumor stem cells that are maintained in a dormant state in this niche. However, the initial challenge posed was to quantify this population in AML patients following allogeneic stem cell transplantation, because the occult population of leukemic myeloblasts can be differentiated from the normal donor hematopoietic elements using genetic tools, especially next generation sequencing.

No expenditures have been made for this program for the last year. This is primarily because of a transition in Dr. Peiper's laboratory. Dr. Jean-Marc Navenot, who has worked under Dr. Peiper's supervision for over 15 years, left the laboratory to refocus his professional efforts and return to France. This has provided the opportunity to extend the scope of the project to explore the interaction of breast cancer cells with supporting stromal cells in collaboration with Dr. Bing-hua Jiang, who has joined the Department of Pathology, Anatomy & Cell Biology and collaborated with Dr. Peiper on multiple publications. The proposed experiments will explore mechanisms responsible for the effect of stromal cells on breast cancer cells, including proliferation, angiogenesis, and metastasis, again focusing on a chemokine-receptor paracrine signaling system, as outlined in the revised specific aims.

Several experiments that have been performed by Dr. Peiper and Dr. Jiang with the involvement of Dr. Ling-Zhi Liu are as follows:

1. Our recent results showed miR-148a acted as tumor suppressors by targeting IGF-IR and IRS1, and downregulation of miR-148a in breast cancer cells was due to the DNA methylation. Interestingly, we also found that levels of miR-148a in CAF cells were more than 10-fold higher than those in breast cancer cells, and more than 8-fold higher than those from the co-cultured breast cancer MB-231 and CAF cells (Fig. 1A). To understand whether the co-culture of MB231 and CAF cells led to significant decrease of miR-148a expression through certain cytokine production, we performed cytokine microarray analysis, and found levels of four secreted cytokines: CXCL1, IL-6, IL-8, MCP-1 and CCL5 in the conditioned medium prepared from the co-culture cells were higher than those prepared from MB-231 or CAF cells alone. The most

dramatic change was levels of CCL5 (data not shown). The mRNA levels of these cytokines in the cells using qRT-PCR analysis showed similar higher levels of CXCL1, IL-6, MCP-1, while CCL5 was 20-fold higher in the co-cultured cells than the BC and CAF cells alone (Fig. 1B). The secreted CCL5 in the co-cultured supernatant was 7-fold higher than BC and CAF cells alone by ELISA assay (Fig. 1C). To determine whether CCL5 results in miR-148a downregulation in CAF cells, we treated CAF cells with CCL5 and found that after the treatment for 4 and 12 h, the miR-148a levels in CAF cells significantly decreased (Fig. 2).

2. Co-culture activated AKT and ERK1/2signaling pathways. Our preliminary data showed that CCL5 treatment suppressed CAF miR-148a expression (Fig. 2). To study whether miR-148 downregulation in CAF is due to CCL5 induction and secretion in the co-cultured cells, we used neutralized antibody against CCL5 in the co-culture of MB-231 and MCF7 with CAF cells and tested miR-148a expression by qRT-PCR similarly as Fig. 2. Our preliminary data (Figs. 1B and 1C) suggest that the interaction between cancer cells and CAF increases CCL5 expression. We knocked down CCL5 expression in BC cells and CAF cells using siRNAs, respectively, to see whether it affects CCL5 secretion and miR-148a expression in the co-culture. Only a little information is available for CCL5 regulation. Previous studies demonstrated that CCL5 could be transcriptionally induced by c-Jun in cancer cells and stromal cells. We found that AKT and ERK1/2 were activated under the co-culture (Fig. 3). To examine whether AKT and ERK1/2 are responsible for the increased CCL5 secretion in the co-culture, we tested whether inhibition of AKT and ERK1/2 by their inhibitors, and knockdown of AKT and ERK1/2 using AKT and ERK1/2 siRNAs in BC cells and CAF cells and tested whether these treatments inhibit CCL5 secretion.

3. Our results show stromal miR-148a and CCL5 expression is important for cell proliferation. Our preliminary results showed that co-culture of cancer and CAF cells can inhibit miR-148a expression in CAF cells, and induce CCL5 expression. Co-culture led to faster cell proliferation than culturing BC or CAF cells alone (Fig. 4). These new results stromal miR-148a and CCL5 expression is important for cell proliferation.

4. We show that forced expression of miR-148a in breast cancer cells attenuated cell proliferation. We expressed miR-148a in breast cancer cells, and showed that miR-148a inhibited cell proliferation (Fig. 5).

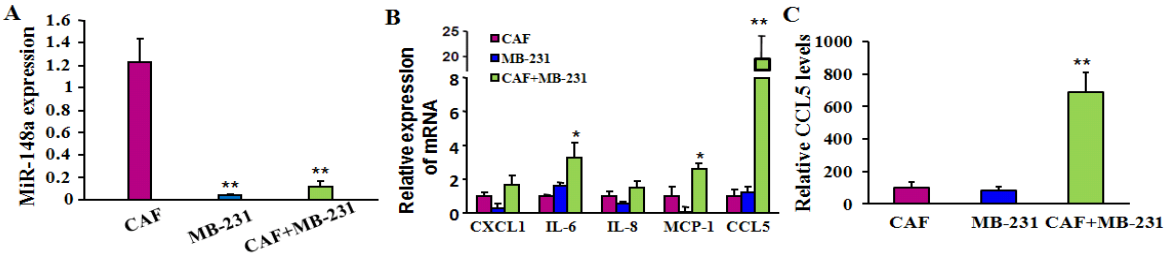

Fig. 1. Co-culture of MDA-MB-231 and stromal CAF cells led to miR-148a downregulation and increased CCL5 secretion. ***A***, CAF, MDA-MB-231 (MB-231) cells, and co-cultured cells (the ratio of CAF to MB231 was 1:2) were seeded in the 6-well plate, After 48 h, miR-148a was tested by qRT-PCR. ***B***, The cells were seeded as above in 6 well plates for 24 h, cells were cultured in serum-free medium for 48 h. Relative expression of CXCL1, IL-6, IL-8, MCP-1 and CCL5 mRNA in each group was determined by real-time PCR. The data represent mean±SD of three independent experiments. * $p<0.05$ and ** $p<0.01$, respectively. ***C***, The conditioned media were collected and subjected to ELISA assay and normalized to the cell number and CAF group. * $p<0.05$. (n=26).

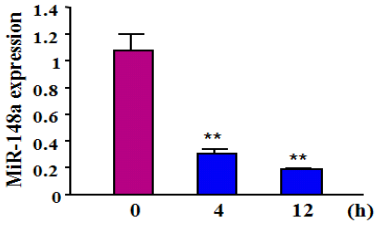

Fig. 2. CCL5 treatment decreased miR-148 expression in CAF cells. CAF cells were treated with CCL5 at 10 ng/ml for 0, 4 and 12 h. MiR-148a was determined by real-time PCR. The data represent mean±SD of three independent experiments. ** $p<0.01$.

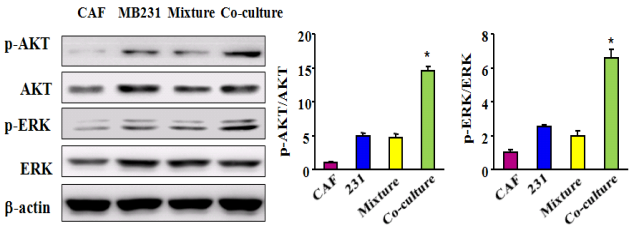

Fig. 3. Co-culture activated AKT and ERK1/2signaling pathways. MDA-MB-231 and CAF cells were co-cultured for 48 h. Cell pellets were subjected to immunoblotting. The data represent mean±SD of three independent experiments. * $p<0.05$.

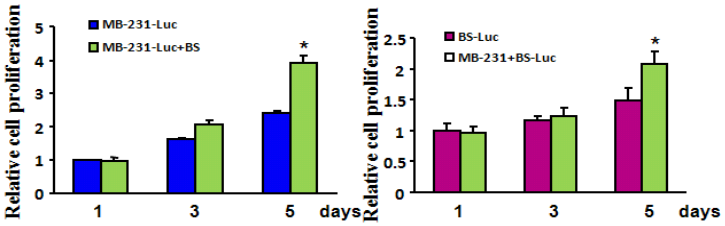

Fig. 4. Co-culture of MB-231 and CAF cells increased proliferation of MB-231 and CAF cells. MDA-MB-231 cells ($3x10^5$) stably expressing Luc construct were seeded alone or with breast stromal CAF cells ($1.5x10^5$) in 6 wells plate (left). $1.5x10^5$ breast stromal cells stably expressing Luc were seeded alone or with $3x10^5$ MDA-MB-231 cells in 6 wells plate (right). The luciferase activities were measured in day 1, 3 and 5 after cell seeded. The data represent mean±SD of three independent experiments. * $p<0.01$.

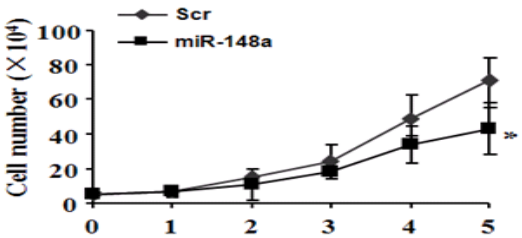

Fig. 5. Forced expression of miR-148a in MB-231 cells suppressed cell proliferation. MB-231 cells were infected with lentivirus carrying scrambled sequence (Scr) or miR-148a, and selected with puromycin to obtain cell lines stably expressing Scr or miR-148a. Cell proliferation assay was performed using the stable cell lines for 5 days (without puromycin) after the seeding.* $p<0.01$.